Chemical Engineering Journal 498 (2024) 155195

Contents lists available at ScienceDirect

Chemical Engineering Journal

journal homepage: www.elsevier.com/locate/cej

Body temperature-triggered adhesive ionic conductive hydrogels for bioelectrical signal monitoring

Xuelan Li [a], Yue Sun [a], Shenglong Wang [a], Guo Tian [a], Tao Yang [a], Longchao Huang [a], Yong Ao [a], Boling Lan [a], Jieling Zhang [a], Tianpei Xu [a], Yang Liu [a], Long Jin [a], Weiqing Yang [a,b], Weili Deng [a,*]

[a] Key Laboratory of Advanced Technologies of Materials (Ministry of Education), School of Materials Science and Engineering, Southwest Jiaotong University, Chengdu 610031, PR China
[b] Research Institute of Frontier Science, Southwest Jiaotong University, Chengdu 610031, PR China

ARTICLE INFO

Keywords:
Hydrogel electrode
Ion-conductive hydrogels
Adhesive hydrogel
Body temperature-triggered
Surface electromyography

ABSTRACT

Bioadhesive ion-conductive hydrogels are essential in bioelectrical signal monitoring. However, highly adhesive hydrogels may cause discomfort, such as skin redness and pain when peeled off, which hinders their application. Here, we design a body temperature-triggered adhesive ionic conductive hydrogel based on biocompatible polyacrylamide (PAAM), gelatin, and sodium alginate (SA). Due to the temperature sensitivity of gelatin, the adhesion of the developed PAAM/gelatin/SA (PGS) hydrogel is rapidly enhanced upon exposure to human body temperature, and it decreases quickly within a short period (10 s) after cooling, thus enabling painless removal. At the same time, the hydrogel exhibits a Young's modulus (~265 kPa) similar to that of skin tissue and achieves a conformal contact to the skin. Benefiting from the low electrode-epidermal impedance, the developed hydrogel has a decent signal-to-noise ratio of about 25 dB, allowing high-fidelity recording of various bioelectrical signals and accurate recognition of movements. The temperature-triggered adhesion-changing conductive hydrogel presented in this work shows great potential for biomedical applications.

1. Introduction

Bioelectrical signals, such as electrocardiogram (ECG), electromyogram (EMG) and electroencephalogram (EEG), serve as the fundamental physiological indicators of the human body, providing valuable insights into the laws of biological movement and the underlying mechanisms of physiological disorders [1–6]. To ensure stable and precise recording of these signals, flexible, wearable, and biocompatible electrodes are essential [7,8]. Currently, most reported bioelectrodes are made by mixing conductive fillers with elastic matrices, such as carbon-based entities (e.g., carbon nanotubes, graphene) [9,10], conductive polymers (e.g., polyaniline, polypyrrole) [11,12], as well as metallic components (e.g., Ag nanowires, liquid metals) [13,14]. For example, Nan Liu and her team prepared a durable and non-disposable transparent graphene skin electrode for detecting electrophysiological signals, by semi-embedding highly graphitized electrospun fibers/monolayer graphene into soft elastomer [15]. The researchers also mixed thermally expandable microspheres with liquid metal nanoparticles to dynamically monitor EMG signals utilizing the conductive pathways between the liquid metal particles [16]. However, such bioelectrodes reported so far are stiff and their Young's modulus (~1 MPa − 1 GPa) is several orders of magnitude higher than that of biological tissues (~100 kPa) [17], resulting in electrode-epidermal impedances typically reaching hundreds of kΩ, which makes it difficult to obtain high-quality bioelectrical signals [18]. Whereas, conductive hydrogels (CHs) exhibit skin-like properties such as a similar Young's modulus, softness and conductivity, thus attracting increasing attention in bioelectrodes [19–21].

Various conductive hydrogels have been developed based on different conductive mechanisms, such as ionic- [22,23], metallic- [24], and polymer- [25] based systems. Among them, ionic conductive hydrogels (ICHs) are particularly attractive due to their biocompatibility, tunable mechanical properties and high electrical conductivity [26–29]. In ion-conducting hydrogels, a high content of free ions can endow the hydrogel with high electrical conductivity, which can greatly reduce the skin contact impedance, and thus capture high-quality

* Corresponding author.
E-mail address: weili1812@swjtu.edu.cn (W. Deng).

https://doi.org/10.1016/j.cej.2024.155195
Received 23 May 2024; Received in revised form 10 August 2024; Accepted 24 August 2024
Available online 27 August 2024

electrical signals. Meanwhile, the introduction of ions can improve the water retention of the hydrogel, which is important for achieving long-term stable monitoring of bioelectrical signals [30,31].

In addition to electrical conductivity, adhesion is another essential property of flexible bioelectrode. Tight adhesion during monitoring ensures precise electrical signal capture, while weak adhesion during peeling minimizes discomfort or skin damage for the user. Therefore, such on-demand peeling places higher demands on the controlled adhesion of the hydrogel. Adhesive hydrogels can be achieved by changing the chemical composition or surface groups with the help of complementary functional groups (carbon–carbon, carbon–nitrogen, siloxanes, amides, etc.) [32,33] and physical interactions (e.g., ionic bonding, hydrogen bonding, van der Waals forces, etc.) [34,35]. Triggerable detachment of hydrogels can be achieved by cleaving non-covalent or covalent bonds through various stimuli such as chemical reagents, light, pH, electrical stimulation, or heat [36–40]. For example, Xu et al. successfully prepared a nanocellulose/polyacrylic acid hydrogel (CNF/PAA) with a tight hydrogen bonding network using enolate monomer and nanocellulose. The pH change of sweat was utilized to promote the generation of protonation and the decoupling of the hydrogel hydrogen-bonding network, thus releasing more free and reactive hydrophilic groups and achieving dynamic adhesion of the hydrogel [41]. Researchers have proposed a PAA/Fe/Li hydrogel with electrically programmable adhesion, in which an external electric field was used to precisely control the spatiotemporal dynamics of ion diffusion to achieve dynamic adhesion of the hydrogel [42]. However, controlling the dynamic adhesion of hydrogel by these methods is not only triggered by harsh conditions but also has a long response time. The temperature-controlled hydrogel can trigger the dynamic adhesion of the hydrogel through the human body temperature, which can greatly shorten the response time for various application scenarios.

Here, we demonstrate a polyacrylamide/gelatin/sodium alginate/lithium chloride ionic hydrogel for monitoring bioelectrical signals. The introduction of gelatin and sodium alginate into polyacrylamide hydrogels significantly improves the mechanical properties of the hydrogels (elongation 800 %). Meanwhile, due to the temperature-controlled reversible phase transition property of gelatin [43], the helical structure of gelatin collagen fibers unfolds when heated and self-assembles into a helical structure when cooled [44], which provides a basis for designing temperature-triggered adhesive hydrogels. The experimental results show that the adhesion of the developed ionic hydrogel can be changed rapidly in a short period of time, enabling painless peeling. In addition, for bioelectrical signal monitoring, the ionic hydrogel shows a high signal-to-noise ratio of about 25 dB, which is comparable to that of commercial bioelectrodes (~26 dB), allowing accurate acquisition of surface EMG signals and assessment of muscle status.

2. Experimental section

2.1. Materials

Gelatin (medical grade, gel strength ~ 250 g bloom), acrylamide (AAm, AR, 99.9 %), sodium alginate (SA), lithium chloride (LiCl, 99.5 %), N,N′-Methylenebis (acrylamide) (MBAA, 99 %), N,N,N′,N′-Tetramethylethylenediamine (TEMED, 99 %) and ammonium persulfate (APS, 99.99 %) were all purchased from Aladdin reagent Inc. and used without further purification.

2.2. Preparation of PGS hydrogel

First, 5 wt% gelatin and 0.8 wt% sodium alginate were dissolved in 20 mL of deionized water in a water bath at 60 °C, maintaining stirring until completely dissolved. After the solution was cooled to room temperature, 20 wt% acrylamide was added and stirred thoroughly until homogeneous. Next, 0.01 g of MBAA and 250 μL of APS were added to this mixed solution, and possible air bubbles were removed by sonication. Finally, 20 μL TEMED was added to induce polymerization of the hydrogel, which was immediately poured into a pre-prepared mold to form a polyacrylamide/gelatin/sodium alginate (PGS) composite hydrogel.

2.3. Hydrogel adhesion test

The tissue adhesion strength of different hydrogels was determined by the adhesion-tension test, in which hydrogels (25 mm*25 mm*2 mm) were first applied to various substrates and preloaded with a pressure of 20 N for 10 s. The experimental samples were then pulled using a UTM (Instron 5567, USA) at a crosshead speed of 5 mm min^{-1} until the samples were separated from the substrate at different temperatures. Each hydrogel was tested 3 times on different substrates and the adhesion strength was calculated by dividing the maximum load by the initial contact area.

2.4. Characterization

SEM and EDS images were observed using a scanning electron microscope (SEM, JSM-7800) with an accelerating voltage of 5 kV. Optical images were taken by a stereo photomicrographic microscope (Saike-digital). The chain structure of the hydrogels was characterized using Fourier transform infrared spectroscopy (FT-IR, Nicolet IS50 spectrometer). Tensile and compression tests: Hydrogels (50 mm*8.5 mm*2 mm) made in the shape of dumbbells were pulled by a universal testing machine (UTM, Instron 5567, USA) at a crosshead speed of 10 mm min^{-1} to perform the tensile test of the hydrogels. Compression test: Cylindrical hydrogel specimens of 11 mm in height and 10 mm in diameter were compressed using a universal testing machine with a crosshead speed of 5 mm min^{-1}. The dynamic rheological tests of PGS hydrogels were carried out using a rotational rheometer (TA DHR-1, USA) equipped with 25 mm parallel plates at a frequency of 10 Hz and a strain amplitude of 1.0 % over a temperature range of 25 to 40 °C. Nyquist, electrical conductivity and contact impedance of the hydrogels (20 mm*20 mm*5 mm) were measured by an electrochemical workstation (CH Instruments, CHI660E). The electrical conductivity was calculated by the following equation.

$$\text{Conductivity}\,(\text{S/m}) = \frac{\text{Length}\,(\text{m})}{\text{resistance}\,(\Omega)\ \times \text{crosssectionalarea}\,(\text{m}^2)}$$

3. Results and discussion

3.1. Design and fabrication of PGS hydrogels

Acrylamide (AAm), gelatin, and sodium alginate (SA) were dissolved in deionized water at 60 °C, and PGS hydrogels were formed by free radical-initiated polymerization using MBAA as a chemical cross-linking agent, APS as an initiator, and TEMED as a promoter (**Fig. S1**). The covalently crosslinked PAAM chains provide a strong chemical bonding network for the hydrogel, in which gelatin and PAAM interact with each other through hydrogen bonding to form an interpenetrating dual-network structure, while a small amount of SA is uniformly dispersed in the dual-network through inter- and intramolecular hydrogen bonding, thus improving the mechanical properties of the hydrogel. Adding lithium chloride (LiCl) provides many free ions to the hydrogel, constructing abundant pathways for the conduction of electrical signals (Fig. 1**a**). With an increase in temperature to 37 °C, the hydrogen bonding in gelatin is weakened, and the triple helix of gelatin unfolds and exposes amino, hydroxyl, and carboxyl groups, resulting in the formation of multiple interfacial bonds at the interface between the PGS hydrogel and the skin surface to achieve stronger adhesion. In contrast, as the temperature decreases to 25 °C, the gelatin chains re-twine and the interfacial bonding with the skin surface is weakened, resulting in a

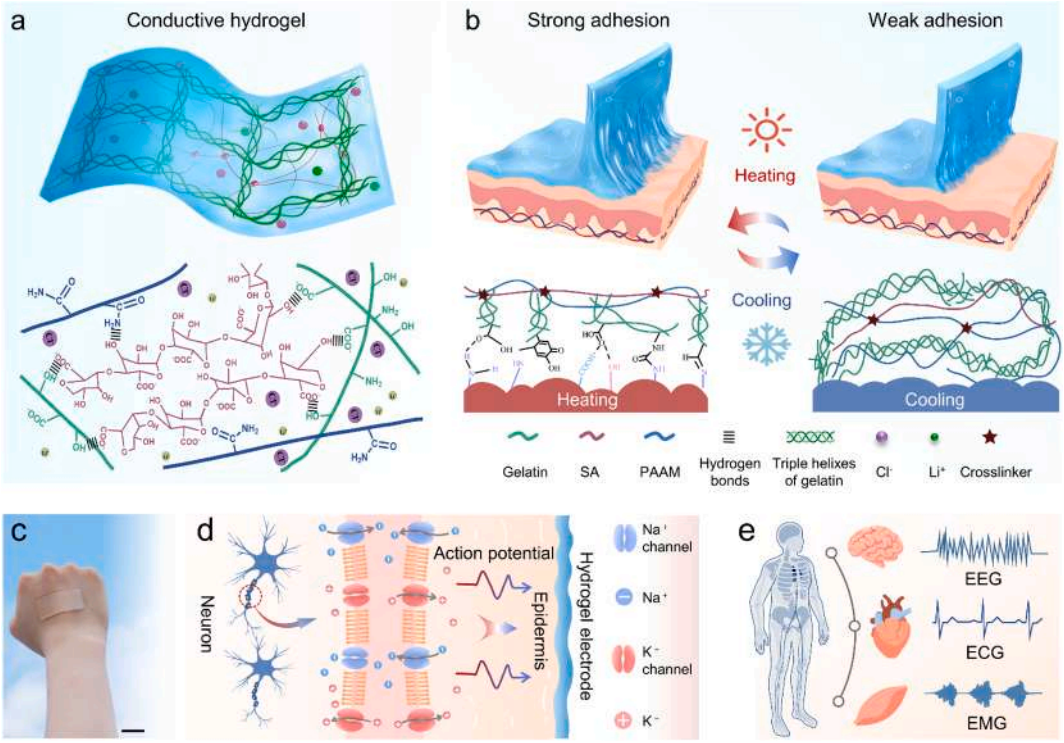

Fig. 1. Schematic diagram of PGS hydrogel with temperature-regulated adhesion. a) PGS conductive hydrogel and its network structure. b) Schematic diagram of PGS hydrogel body temperature-triggered adhesion and ice-cold-induced painless detachment. c) Optical picture of PGS hydrogel. Scale bar: 2 cm. d) Schematic diagram of myoelectric signaling conduction through hydrogel. e) Potential applications of the PGS hydrogel for monitoring bioelectrical signals (ECG, EMG, and EEG).

non-destructive separation of the hydrogel from the skin surface [45,46]. Thus, the PGS hydrogels achieve temperature-regulated adhesion to the skin (Fig. 1**b**). Additionally, the hydrogel is sufficiently transparent and flexible to easily form a conformal contact with the skin surface (Fig. 1**c**).

When muscles are active, action potentials can be generated by opening and closing sodium and potassium ion channels. In the initial phase, sodium channels open and sodium ions flow into the cell, leading to depolarization, followed by sodium channels closing and potassium channels opening and potassium ions flowing out of the cell to achieve repolarization. This process not only expresses changes in potential but also causes local differences in charge distribution (**Fig. S2**). PGS hydrogel electrodes attached on the skin surface could convert these changes through the skin-electrode interface, enabling the acquisition of electrical signals (Fig. 1**d**) [47–50]. On this basis, the PGS hydrogel electrode allows for the acquisition of complex bioelectrical signals, such as EMG, ECG, EEG, for medical diagnostics and physiological research (Fig. 1**e**).

3.2. Mechanical properties of PGS hydrogels

With the addition of SA, a more complex network structure between PAAM/gelatin and SA was formed through hydrogen bonding and electrostatic interactions between molecular chains to regulate the morphology and properties of the hydrogel (Fig. 2**a**). Observing the microstructure of the hydrogel by SEM, it can be found that the pores of pure PAAM are large, with thick and inhomogeneous pore walls, whereas the structure of the hydrogel becomes relatively dense after the addition of gelatin, which indicates that the interactions between the components are strengthened. After further addition of SA, the pores become more uniform and the pore density increases significantly, showing a denser crosslinked structure, which is conducive to improving the mechanical strength and electrical conductivity of the hydrogel (Fig. 2**b**). In addition, EDS studies of the PGS ion-conducting hydrogel show that Na, Li, and Cl elements are uniformly distributed in the three-dimensional network of the hydrogel (**Fig. S3**).

Tensile and compression testing can help determine the strength of hydrogels under tension, bending and compression. In practice, hydrogels may be subjected to tensile forces in applications such as fingers, wrists and other joints. If the tensile strength is insufficient, the gel may rupture during use, leading to bond failure. Therefore, the mechanical properties of hydrogels are also important for their application. The tensile stress–strain curves of PGS hydrogels with various SA contents are shown in Fig. 2**c**. It can be found that when the SA content increases from 0 to 0.8 wt%, the tensile stress of the hydrogel increases from 61.3 kPa to 229.3 kPa, the elongation at break increases from 428.4 % to 706.4 % (Fig. 2**d**), the work of rupture increases from 0.1 MJ/m^3 to 0.7 MJ/m^3 (**Fig. S4**), and Young's modulus increases from 107.2 kPa to 265.9 kPa (Fig. 2**e**). These improved performances are mainly attributed to the introduction of SA, which leads to the formation of hydrogen bonds or an increase in chain density. However, when the SA concentration continued to increase to 1 wt%, the mechanical properties of PGS hydrogels begin to decay. This is because excessive SA addition leads to an uneven structural distribution of PGS hydrogels and affects their mechanical properties. In addition, from the stress–strain curves of hydrogels with different gelatin contents (**Fig. S5**), the variation of gelatin content has little effect on the mechanical properties of the hydrogels. From the consecutive tensile cycling tests performed at the same elongation of 400 %, it can be seen that the hysteresis loops basically overlap except for the first one, indicating the good resilience of the hydrogel (Fig. 2**f**). Similarly, the compressive properties of PGS hydrogels were improved by the doping of SA. Compared to the PAAM/gelatin hydrogel (2.6 kPa), the PGS hydrogel achieves a compressive stress of 3.4 kPa at 80 % strain (**Fig. S6a-b**). Evaluating the loading–unloading compression of the hydrogels at 70 % strain (**Fig. S6c**), the PGS hydrogels show less energy consumption in the first cycle, and

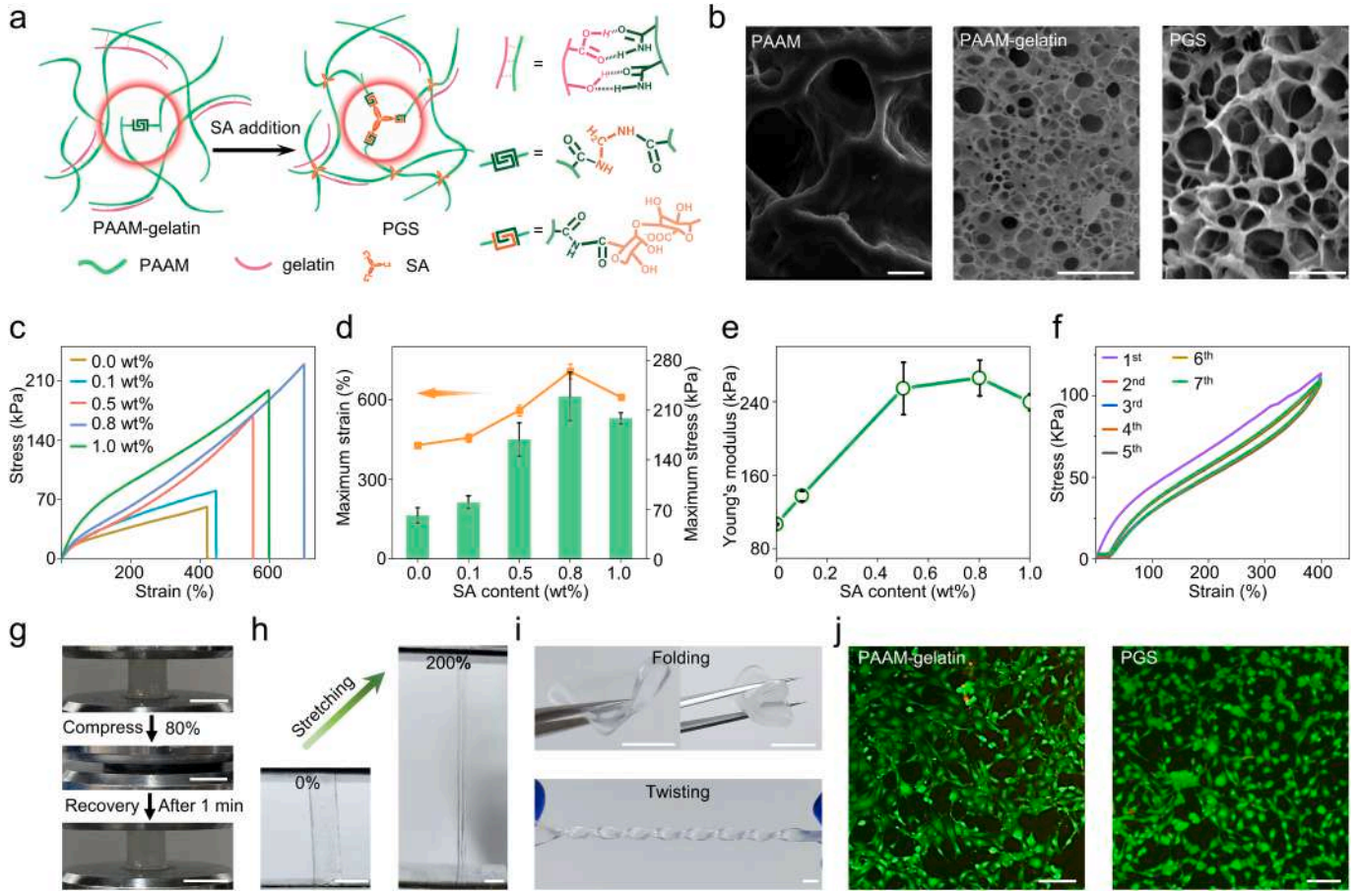

Fig. 2. Characterization and mechanical properties of PGS hydrogel. a) Schematic structures of PAAM/gelatin and PGS hydrogels. With the addition of SA, the PAAM/gelatin chains are cross-linked with SA to form a porous structure. b) SEM images of PAAM, PAAM/gelatin and PGS hydrogels. All scale bars are 10 μm. Tensile curves (c), maximum stress and strain (d), Young's modulus (e) of hydrogels with different SA contents. f) Cyclic tensile curves of hydrogels at 400 % strain. g) Optical images of PGS during compression and after recovery. All scale bars are 10 mm. h-i) Optical images of PGS in the stretched, bent and twisted states. All scale bars are 10 mm. j) Live/dead staining results L929 fibroblasts cultured on PAAM-gelatin and PGS hydrogels after 24 h. Live cells are stained green and dead cells are stained red. All scale bars are 100 μm.

the stress–strain curves almost overlapped in the 2nd-10th cycles. As shown in Fig. 2**g**, the PGS hydrogel can withstand a high compressive deformation of 80 % without any damage, and can quickly recover its original shape after removing the load. Meanwhile, the hydrogel can retain its original shape without fracture after being stretched, bent and twisted, as shown in Fig. 2**h-i**. From the cytocompatibility test on L929 mouse fibroblasts, the PGS hydrogel shows better biocompatibility compared to the PAAM/gelatin hydrogel (Fig. 2**j**).

3.3. Body temperature triggered adhesion and painless separation by freezing

Gelatin is a temperature-sensitive protein with a unique triple-helical structure that is extremely sensitive to temperature changes and is thermoreversible. At low temperature, the triple-helix structure is held firmly between molecules, forming gels through aggregation. As the temperature increases, these triple-helical structures disintegrate and convert to single chains. This process results in the exposure of numerous side groups in the gelatin chain, which facilitates the interaction of gelatin with other components of the skin surface, significantly enhancing its adhesion to the skin through non-covalent bonds such as hydrogen bonding or van der Waals forces (Fig. 3**a**). The FT-IR spectra (**Fig. S7**) exhibit a reduction in the absorption peak at 3293 cm^{-1} when the temperature increased from 25 °C to 37 °C, indicating the denaturation of the collagen triple helix structure [51]. Additionally, the absorption peak at 1643 cm^{-1} shifts to a lower wavenumber suggesting the transition of gelatin from a helical to a random coil structure, which enhances the exposure of side groups in the gelatin chains and promotes adhesion to the skin [52]. As the temperature decreases again, the spectra approach the initial curve, indicating that the assembly and derotation of the gelatin helical structure are reversible. Meanwhile, the rheological test results show that the storage modulus (G') of the PGS hydrogel is significantly higher than the loss modulus (G'') at a low temperature of 25 °C, indicating that the elasticity of the hydrogel is dominant at low temperatures, whereas with the increase of temperature, the G' decreased, and the PGS hydrogel exhibits obvious viscoelasticity (**Fig. S8**). At room temperature, PGS hydrogels are difficult to adhere to other surfaces; surprisingly, skin temperature can trigger adhesion (**Fig. S9 and Movie S1**). Once in contact with the skin, the PGS hydrogel is able to form a strong adhesion. By cooling the PGS hydrogel with an ice pack for 10 s, painless detachment from the skin could be achieved (Fig. 3**b**). In contrast, the commercial Ag/AgCl electrodes adhere more strongly to the skin and are often painful to peel off (Fig. 3**c**). This is also confirmed by the greater force required for commercial electrodes in the peeling experiments (Fig. 3**d**). From the simulation results of PGS hydrogel adhesion with temperature, it can be seen that the adhesion of PGS hydrogel increases significantly when the temperature increased from 25 °C to 37 °C, and showed a strong pulling effect (Fig. 3**e**). On the contrary, at a lower temperature of 25 °C, the PGS hydrogel can be easily peeled off from the skin surface with little tensile force, indicating a weak adhesion. This result proves the thermoreversible property of PGS hydrogel: its adhesion can be effectively

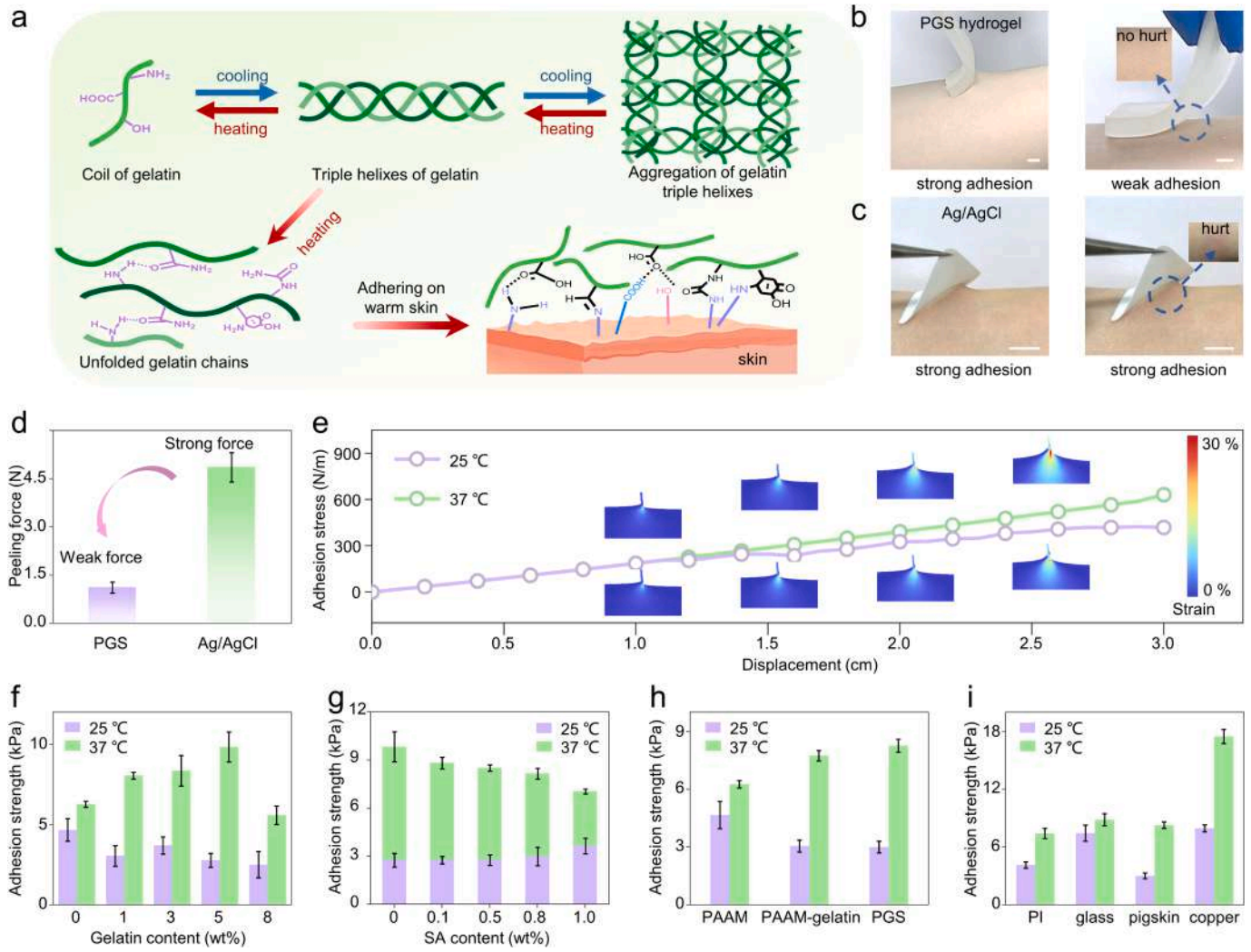

Fig. 3. Mechanisms of body temperature-triggered PGS hydrogel. a) Temperature-induced structural transformation of gelatin chains and adhesion mechanism. b) Photographs of strong adhesion (left) and painless peeling (right) of PGS hydrogel on skin. All scale bars are 5 mm. c) Photographs of strong adhesion (left) and hurt (right) caused by commercial Ag/AgCl electrode during detachment from the skin. All scale bars are 3 cm. d) Peeling force of PGS hydrogel and commercial Ag/AgCl electrode on skin. e) Simulation of strain distribution in vertical peeling of PGS hydrogel at different temperatures. f) Adhesion strength of hydrogels with different gelatin contents to pig skin at different temperatures. g) Adhesion strength of hydrogels with different SA contents to pig skin at different temperatures. h) Comparison of the adhesion strength between PGS, PAAM/gelatin, and pure PAAM hydrogel to pig skin. i) Peeling of PGS hydrogel from different substrates at different temperatures.

triggered by temperature to realize the tunable adhesion.

In investigating the effect of hydrogel composition on its adhesion properties, we observed that the hydrogel exhibited the maximum adhesion force of 9.8 kPa when the gelatin content was 5 wt% (Fig. 3**f**). And the addition of SA slightly decreased the adhesion force of the hydrogel at 37 °C (Fig. 3**g**), which could be attributed to the enhancement of intermolecular forces by the addition of SA. By comparing the adhesion of pure PAAM, PAAM/gelatin complex and PGS hydrogel on pig skin, it is found that PGS hydrogel demonstrates superior adhesion strength (Fig. 3**h**). At room temperature, the hydrogels show poor adhesion to various substrates, including glass, polyimide (PI) and copper foil. However, there is a significant improvement in the adhesion of the hydrogels at 37 °C (Fig. 3**i**), a result that further confirms the significant effect of temperature on the adhesion of hydrogels and also highlights the important role of the material composition on its temperature-responsive behavior. Furthermore, five cyclic adhesion tests of PGS hydrogel under different temperatures show that the hydrogel maintains a high average adhesion strength (9 kPa) at 37 °C and exhibits a low adhesion strength at 25 °C (**Fig. S10**), suggesting a stable temperature-triggered cyclic adhesion of PGS hydrogel.

3.4. Conductivity of PGS hydrogels

The ions of LiCl are free to shuttle through the network structure of PGS hydrogels, and the flow of these ions imparts the hydrogel conductivity (Fig. 4**a**). According to the Nyquist curve in Fig. 4**b**, the electrical conductivity of the PGS hydrogel increases significantly with the content of LiCl, from 0.28 ± 0.008 S m^{-1} to 5.69 ± 0.196 S m^{-1}, which is sufficient to effectively monitor bioelectrical signals (Fig. 4**c**). Unless otherwise stated, hydrogels with 3.5 mol L^{-1} LiCl were used in the following experiments. The excellent conductivity of the PGS hydrogel was further demonstrated by using it as a circuit connecting wire. The brightness of the light-emitting diode is virtually indistinguishable from the result of the metal wire conduction (Fig. 4**d**). The water loss experiments indicate that the water loss rate of the PGS hydrogels gradually decreases with the increase of LiCl content. When the LiCl content reaches 3.5 mol L^{-1}, the water retention rate remained above 60 % on the 7th day (Fig. 4**e**). The reduction of water decreases the electrical conductivity of the PGS hydrogels (Fig. 4**f**), but even so, the conductivity of the PGS hydrogel is still sufficient to conduct the diode after placing for 7 days (**Fig. S11**). In addition, the conductivity of the PGS hydrogel

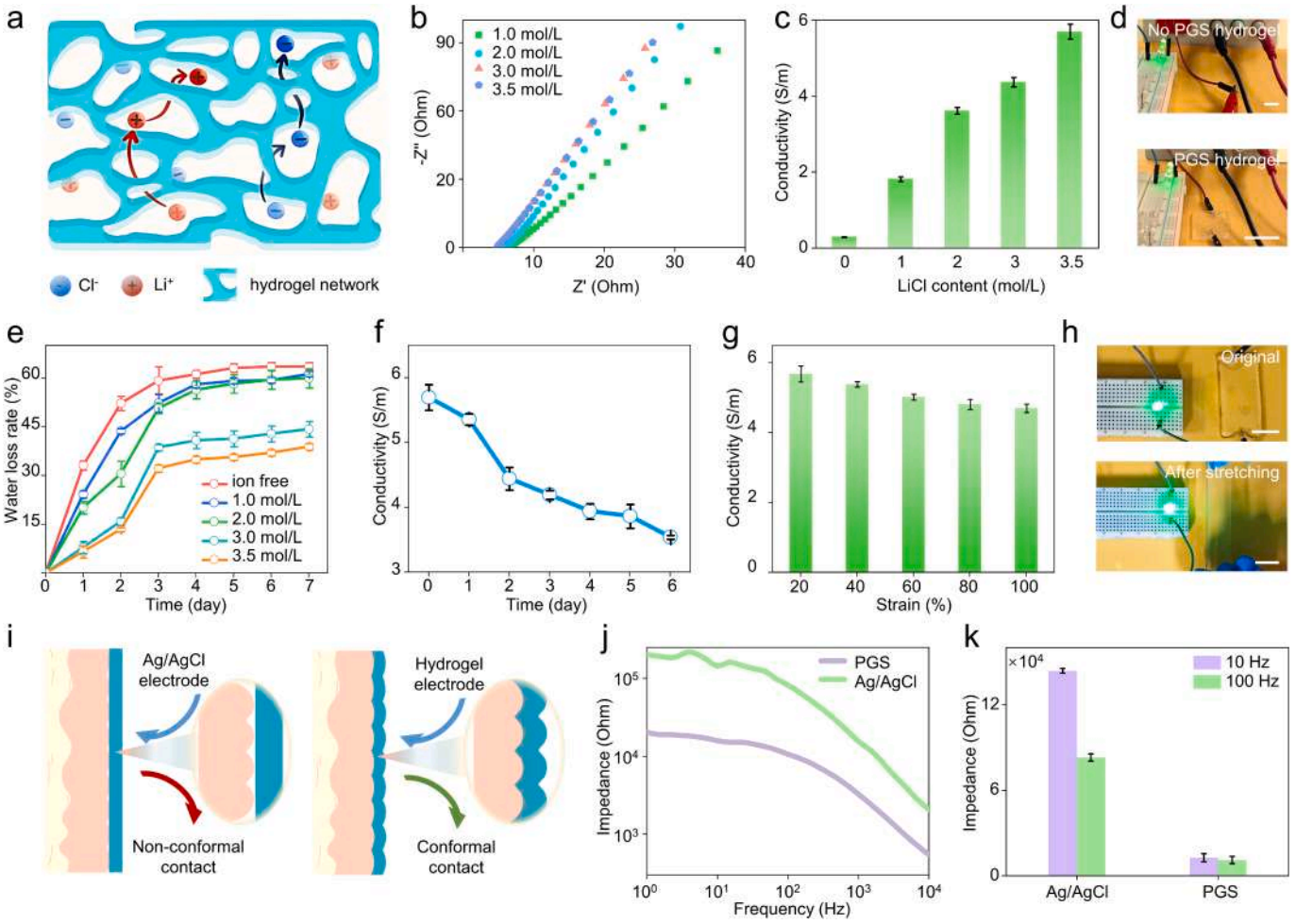

Fig. 4. Conductivity properties and stability of PGS hydrogels. a) Conductive mechanism of Li^+ and Cl^- in the PGS hydrogel network. b) Nyquist plots of PGS hydrogels. c) Conductivity of PGS hydrogels with different LiCl contents. d) Comparison of light-emitting diode luminance with and without PGS hydrogel. All scale bars are 2 cm. e) Water loss of PGS hydrogel with different LiCl contents in 7 days. f) Conductivity changes of PGS hydrogel in 7 days. g) Conductivity of PGS hydrogel under different strain. h) Photograph of light-emitting diode brightness during stretching of PGS hydrogel. All scale bars are 2 cm. i) Schematic diagram of Ag/AgCl electrode and PGS hydrogel electrode in contact with skin. j) Contact impedance between the commercial Ag/AgCl electrode, PGS hydrogel electrode, and human skin from 1 Hz to 10000 Hz. k) Contact impedance of Ag/AgCl and PGS hydrogel electrodes with the human skin at 10 Hz and 100 Hz.

also does not change much under different stretching conditions (Fig. 4**g**), and the brightness of the light-emitting diode connected to the PGS hydrogel remained almost unchanged even when the PGS hydrogel was stretched by 20% (Fig. 4**h**). Furthermore, the conductivity of ion-conducting hydrogels is closely related to temperature [53], as shown in **Fig. S12**, where the conductivity of PGS hydrogels increases with increasing temperature. This not only resultes in enhanced adhesion of PGS after heat triggering, but also improves electrical conductivity, which is more favorable for acquiring electrophysiological signals.

The contact area between the electrode and the skin is the main determinant of the skin-electrode contact impedance [54,55]. Although the commercial Ag/AgCl electrode forms a stronger adhesion to the skin, the contact impedance is high due to the great modulus, resulting in a large contact gap between the electrode and skin. In contrast, the PGS hydrogel is able to achieve tight conformal contact with the skin, eliminating the effect of the gap on impedance and enhancing the conduction of bioelectrical signals (Fig. 4**i** and **Fig. S13**). Contact impedance testing of the PGS hydrogel and commercial Ag/AgCl electrodes shows a gradual decrease in impedance as the frequency increases. However, the PGS hydrogel exhibits lower impedance over the full measurement frequency range (Fig. 4**j**). At 10 Hz and 100 Hz, the contact impedance of the PGS hydrogel decreases by 13×10^4 Ω and 7×10^4 Ω compared to the Ag/AgCl electrode, respectively (Fig. 4**k**). Moreover, PGS hydrogels exhibit adjustable adhesion and good electrical conductivity compared to other hydrogels (**Table S1**). Therefore, the developed PGS hydrogel is more suitable for monitoring electrophysiological signals such as EMG and ECG.

3.5. PGS hydrogel electrodes for sEMG signals monitoring

A systematic diagram of the EMG signals recorded with the PGS hydrogel electrode is shown in Fig. 5**a**. During muscle activity, the superposition of electrical signals from the excited neurons generates local field potentials that convey information about many cells' collective activity, which can be detected and captured by the PGS hydrogel. Compared with commercial Ag/AgCl electrodes, the PGS hydrogel can fit well on large curved fingers and hairy skin (Fig. 5**b**), thus improving the quality of the acquired electrophysiological signals. Meanwhile, the PGS hydrogel electrode does not cause skin redness or swelling after a period of use, which greatly enhances user comfort and safety (Fig. 5**c**). The EMG signals were monitored using PGS hydrogel electrodes and commercial Ag/AgCl electrodes, respectively. From the results, the signal-to-noise ratio (SNR) of the PGS hydrogel electrodes is about 25 dB, comparable to that of the commercial electrodes (Fig. 5**d-e**). The characteristic peaks (P, Q, R, S, T, U) of the ECG signals obtained from the PGS hydrogel could also be clearly distinguished, which lays the

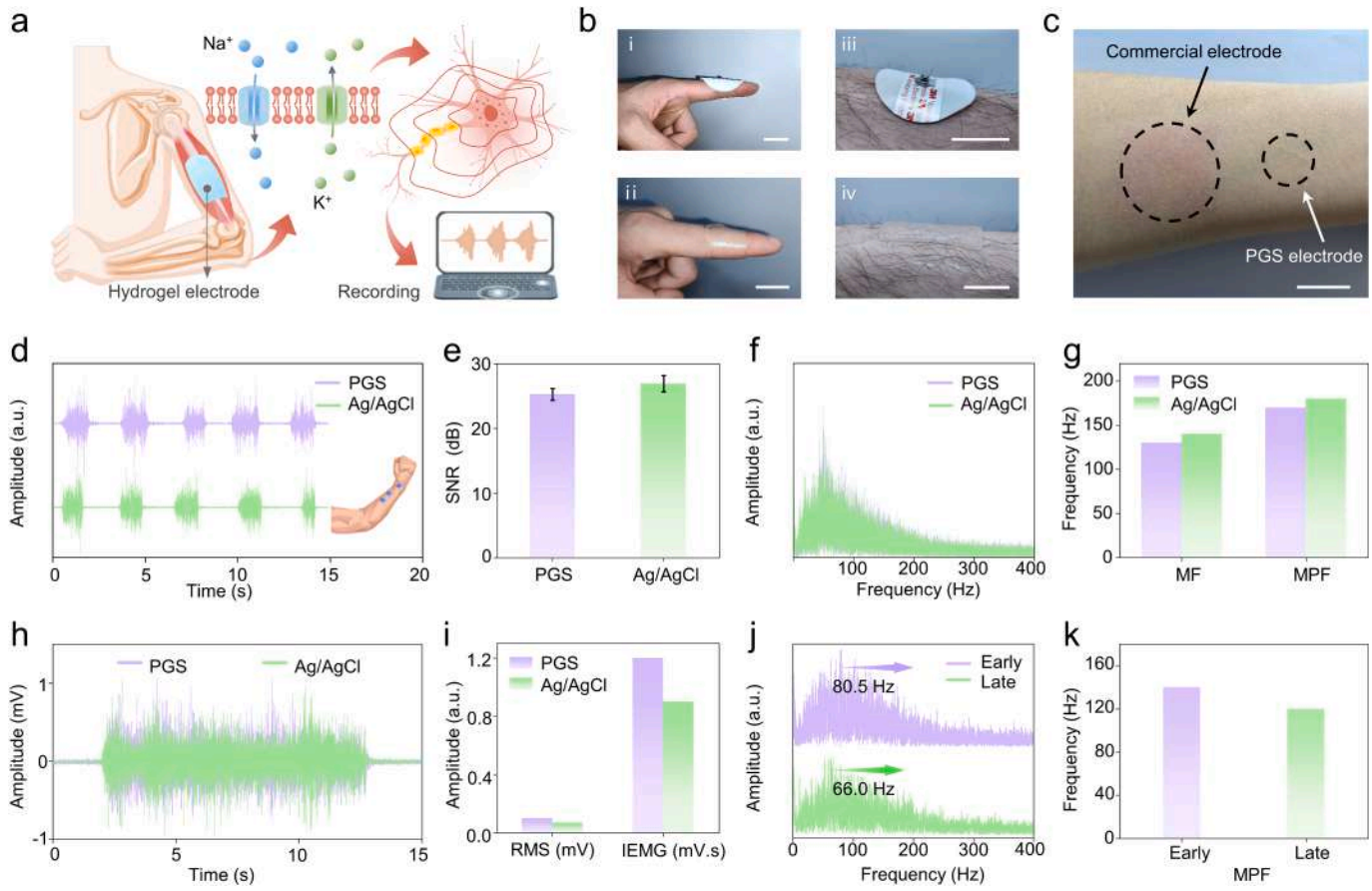

Fig. 5. Application of PGS hydrogel as the myoelectric electrode. a) Schematic diagram of the sEMG acquisition mechanism by PGS hydrogel electrode. b) Photographs of the commercial Ag/AgCl electrode (i, iii) and the PGS hydrogel electrode (ii, iv) on large curvature finger and hairy skin, which show that the PGS hydrogel fits more closely to various types of skin. All scale bars are 2 cm. c) The degree of skin damage caused by the commercial Ag/AgCl electrode and the PGS hydrogel electrodes in practical applications. Scale bar: 2 cm. The sEMG (d), their signal-to-noise ratio (e), frequency spectrum (f) and their mean frequency (MF) and mean power frequency (MPF) (g) recorded by the PGS hydrogel and Ag/AgCl electrodes during fist clenching. The sEMG (h) and time-domain frequency (i) recorded by the PGS and Ag/AgCl electrodes during continuous fist clenching. FFT (j) and MPF (k) changes of sEMG in early and late fatigue stages.

foundation for subsequent practical applications (**Fig. S14**).

Frequency domain and time domain analysis are the most common methods for EMG signals analysis. Information about neuromuscular status can be obtained by converting EMG time-domain signals to frequency-domain signals through the Fourier transform. Fig. 5**f** shows that the major frequencies of the EMG signals acquired by PGS electrode and Ag/AgCl electrode are concentrated in the range of 20–150 Hz; meanwhile, the mean power frequency (MPF) and median frequency (MF) of both signals are not much different from each other (Fig. 5**g**). In time-domain feature metrics, RMS usually reflects the root mean square of EMG, while integrated electromyography (IEMG) reflects the activity state of the muscle [56]. The EMG signals of a sustained clenched fist were recorded by the PGS and Ag/AgCl electrodes, respectively. It can be found that the RMS and IEMG from the PGS electrode were slightly higher than those from the Ag/AgCl electrode (Fig. 5**h-i**). The above results indicate that the PGS hydrogel electrode can accurately monitor a variety of electrophysiological signals, which provides a possible pathway for wearable medicine. On this basis, we demonstrate the potential of PGS hydrogel electrodes to analyze muscle fatigue, one of the most significant causes of sport injuries [57]. Specifically, subjects repeated 20 repetitions of isotonic and isometric contractions and acquired surface EMG (sEMG) signals with the PGS electrode (**Fig. S15**). Fast Fourier transform (FFT) analysis of the sEMG signals of early fatigue (0–15 s) and late fatigue (40–55 s) reveal that the FFT peak frequency of the late fatigue sEMG signal (66 Hz) is significantly lower than that of the early fatigue sEMG signal (80.5 Hz), as shown in Fig. 5**j**. Meanwhile, the mean power frequency (MPF) of the sEMG signal decreases in the late phase of the exercise, which is a typical feature of muscle fatigue (Fig. 5**k**). The PGS hydrogel electrodes exhibit excellent performance in determining muscle fatigue, which has a broad application prospect for monitoring and evaluating various complex conditions of muscles.

4. Conclusion

In summary, the polyacrylamide/gelatin/sodium alginate ion-conducting hydrogel proposed in this study exhibits decent performance for monitoring EMG signals, ECG signals, etc. The developed PGS hydrogel can trigger a stable adhesion to the skin at body temperature (37 °C), and can be easily peeled off after cold compressing for about 10 s, without causing damage to the skin. The PGS hydrogel exhibits excellent electrical conductivity (5.69 S m^{-1}) and flexibility (can adhere well to various skin surfaces), which reduces the contact impedance with the skin and enables high-quality sEMG signal acquisition with a SNR of 25 dB. This study provides a promising opportunity to design temperature-triggered hydrogels, which show great potential for applications in constructing reliable biological interfaces and high-fidelity recording of bioelectrical signals.

CRediT authorship contribution statement

Xuelan Li: Writing – original draft, Visualization, Validation, Data curation, Conceptualization. **Yue Sun:** Writing – review & editing,

Validation, Software. **Shenglong Wang:** Writing – review & editing, Resources. **Guo Tian:** Writing – review & editing, Visualization. **Tao Yang:** Writing – review & editing, Resources. **Longchao Huang:** Software, Resources, Data curation. **Yong Ao:** Resources. **Boling Lan:** Supervision, Software. **Jieling Zhang:** Software. **Tianpei Xu:** Validation. **Yang Liu:** Supervision, Software. **Long Jin:** Validation, Resources. **Weiqing Yang:** Writing – review & editing, Funding acquisition. **Weili Deng:** Writing – review & editing, Supervision, Investigation, Funding acquisition, Conceptualization.

Declaration of competing interest

The authors declare that they have no known competing financial interests or personal relationships that could have appeared to influence the work reported in this paper.

Data availability

Data will be made available on request.

Acknowledgments

The authors acknowledge the National Natural Science Foundation of Sichuan Province of China (No. 2023NSFSC0313), the National Natural Science Foundation of China (No. U2330120), the Basic Research Cultivation Project of Southwest Jiaotong University (No. 2682023KJ024). The authors also want to thank the full support from the Analysis and Testing Center of Southwest Jiaotong University.

Appendix A. Supplementary data

Supplementary data to this article can be found online at https://doi.org/10.1016/j.cej.2024.155195.

References

[1] W. Liu, R.J. Xie, J.Y. Zhu, J.S. Wu, J.F. Hui, et al., A temperature responsive adhesive hydrogel for fabrication of flexible electronic sensors, npj Flex, Electron. 6 (1) (2022) 68, https://doi.org/10.1038/s41528-022-00193-5.
[2] C. Sun, J. Luo, T. Jia, C. Hou, Y. Li, et al., Water-resistant and underwater adhesive ion-conducting gel for motion-robust bioelectric monitoring, Chem. Eng. J. 431 (2) (2022) 134012, https://doi.org/10.1016/j.cej.2021.134012.
[3] T.F. Song, W.M. Zheng, P. Song, Z. Cui, EEG emotion recognition using dynamical graph convolutional neural networks, IEEE t. Affect. Comput. 11 (3) (2020) 532–541, https://doi.org/10.1109/Taffc.2018.2817622.
[4] J. Qi, G. Jiang, G. Li, Y. Sun, B. Tao, Surface EMG hand gesture recognition system based on PCA and GRNN, Neural Comput. & Applic. 32 (10) (2019) 6343–6351, https://doi.org/10.1007/s00521-019-04142-8.
[5] J. Luo, Y. Xing, C. Sun, L. Fan, H. Shi, et al., A bio-adhesive ion-conducting organohydrogel as a high-performance non-invasive interface for bioelectronics, Chem. Eng. J. 427 (2022) 130886, https://doi.org/10.1016/j.cej.2021.130886.
[6] U.R. Acharya, H. Fujita, O.S. Lih, Y. Hagiwara, J.H. Tan, et al., Automated detection of arrhythmias using different intervals of tachycardia ECG segments with convolutional neural network, Inf. Sci. 405 (2017) 81–90, https://doi.org/10.1016/j.ins.2017.04.012.
[7] X.R. Ren, S.L. Wang, D. Xiong, G. Tian, B.L. Lan, et al., Heterogeneously assembled bionic piezoresistive sensor for spinal behavior monitoring, Chem. Eng. J. 485 (2024) 149817, https://doi.org/10.1016/j.cej.2024.149817.
[8] G. Tian, W.L. Deng, T. Yang, J.L. Zhang, T.P. Xu, et al., Hierarchical piezoelectric composites for noninvasive continuous cardiovascular monitoring, Adv. Mater. 36 (2024) 2313612, https://doi.org/10.1002/adma.202313612.
[9] S. Xia, S.X. Song, F. Jia, G.H. Gao, A flexible, adhesive and self-healable hydrogel-based wearable strain sensor for human motion and physiological signal monitoring, J. Mater. Chem. B 7 (30) (2019) 4638–4648, https://doi.org/10.1039/c9tb01039d.
[10] H. Moon, J.-W. Jang, S. Park, J.-H. Kim, J.S. Kim, et al., Soft, conformal PDMS-based ECoG electrode array for long-term in vivo applications, Sensor. Actuat. B-Chem. 401 (2024) 135099, https://doi.org/10.1016/j.snb.2023.135099.
[11] Y. Gao, B. Yin, X.B. Liu, S. Wu, Difunctional microelectrode arrays for single-cell electrical stimulation and pH detection, Anal. Chem. 96 (5) (2024) 2087–2093, https://doi.org/10.1021/acs.analchem.3c04766.
[12] S.L. Wang, Y.L. Yao, W.L. Deng, X. Chu, T. Yang, et al., Mass-produced skin-inspired piezoresistive sensing array with interlocking interface for object recognition, ACS Nano 18 (17) (2024) 11183–11192, https://doi.org/10.1021/acsnano.4c00112.
[13] S.W. Wu, L.H. Li, H. Xue, K. Liu, Q.R. Fan, et al., Size controllable, transparent, and flexible 2D silver meshes using recrystallized ice crystals as templates, ACS Nano 11 (10) (2017) 9898–9905, https://doi.org/10.1021/acsnano.7b03821.
[14] K. Le, X. Sun, J. Chen, J.V. John, A. Servati, et al., Stretchable, self-healing, biocompatible, and durable ionogel for continuous wearable strain and physiological signal monitoring, Chem. Eng. J. 471 (2023) 144675, https://doi.org/10.1016/j.cej.2023.144675.
[15] J.K. Qiu, T.H. Yu, W.F. Zhang, Z.H. Zhao, Y. Zhang, et al., A bioinspired, durable, and nondisposable transparent graphene skin electrode for electrophysiological signal detection, ACS Mater. Lett. 2 (8) (2020) 999–1007, https://doi.org/10.1021/acsmaterialslett.0c00203.
[16] Y. Niu, G. Tian, C. Liang, T. Wang, X. Ma, et al., Thermal-sinterable EGaIn nanoparticle inks for highly deformable bioelectrode arrays, Adv. Healthcare Mater. 12 (10) (2023) 2202531, https://doi.org/10.1002/adhm.202202531.
[17] H. Yuk, B.Y. Lu, X.H. Zhao, Hydrogel bioelectronics, Chem. Soc. Rev. 48 (6) (2019) 1642–1667, https://doi.org/10.1039/C8CS00595H.
[18] J. Park, J.Y. Kim, J.H. Heo, Y. Kim, S.A. Kim, et al., Intrinsically nonswellable multifunctional hydrogel with dynamic nanoconfinement networks for robust tissue-adaptable bioelectronics, Adv. Sci. 10 (12) (2023) 2207237, https://doi.org/10.1002/advs.202207237.
[19] D. Gan, Z. Huang, X. Wang, D. Xu, S. Rao, et al., Bioadhesive and electroactive hydrogels for flexible bioelectronics and supercapacitors enabled by a redox-active core-shell PEDOT@PZIF-71 system, Mater. Horiz. 10 (6) (2023) 2169–2180, https://doi.org/10.1039/d2mh01234k.
[20] X. Huang, C. Chen, X. Ma, T. Zhu, W. Ma, et al., In situ forming dual-conductive hydrogels enable conformal, self-adhesive and antibacterial epidermal electrodes, Adv. Funct. Mater. 33 (38) (2023) 2302846, https://doi.org/10.1002/adfm.202302846.
[21] T. Zhou, H. Yuk, F.Q. Hu, J.J. Wu, F.J. Tian, et al., 3D printable high-performance conducting polymer hydrogel for all-hydrogel bioelectronic interfaces, Nat. Mater. 22 (7) (2023) 895–902, https://doi.org/10.1038/s41563-023-01569-2.
[22] X.J. Sui, H.S. Guo, C.C. Cai, Q.S. Li, C.Y. Wen, et al., Ionic conductive hydrogels with long-lasting antifreezing, water retention and self-regeneration abilities, Chem. Eng. J. 419 (2021) 129478, https://doi.org/10.1016/j.cej.2021.129478.
[23] S.H. Wang, L. Yu, S.S. Wang, L. Zhang, L. Chen, et al., Strong, tough, ionic conductive, and freezing-tolerant all-natural hydrogel enabled by cellulose-bentonite coordination interactions, Nat. Commun. 13 (1) (2022) 3408, https://doi.org/10.1038/s41467-022-30224-8.
[24] B. Liu, R. Bo, M. Taheri, I. Di Bernardo, N. Motta, et al., Metal–organic frameworks/conducting polymer hydrogel integrated three-dimensional free-standing monoliths as ultrahigh loading Li–S battery electrodes, Nano Lett. 19 (7) (2019) 4391–4399, https://doi.org/10.1021/acs.nanolett.9b01033.
[25] H. Xu, W. Zheng, Y. Zhang, D. Zhao, L. Wang, et al., A fully integrated, standalone stretchable device platform with in-sensor adaptive machine learning for rehabilitation, Nat. Commun. 14 (1) (2023) 7769, https://doi.org/10.1038/s41467-023-43664-7.
[26] H.L. Huang, L. Han, J.F. Li, X.B. Fu, Y.L. Wang, et al., Super-stretchable, elastic and recoverable ionic conductive hydrogel for wireless wearable, stretchable sensor, J. Mater. Chem. A 8 (20) (2020) 10291–10300, https://doi.org/10.1039/d0ta02902e.
[27] R.A. Li, K.L. Zhang, L. Cai, G.X. Chen, M.H. He, Highly stretchable ionic conducting hydrogels for strain/tactile sensors, Polymer 167 (2019) 154–158, https://doi.org/10.1016/j.polymer.2019.01.038.
[28] K. Shen, K. Xu, M. Zhang, J. Yu, Y. Yang, et al., Multiple hydrogen bonds reinforced conductive hydrogels with robust elasticity and ultra-durability as multifunctional ionic skins, Chem. Eng. J. 451 (1) (2023) 138525, https://doi.org/10.1016/j.cej.2022.138525.
[29] X. Yao, S. Zhang, L. Qian, N. Wei, V. Nica, et al., Super stretchable, self-healing, adhesive ionic conductive hydrogels based on tailor-made ionic liquid for high-performance strain sensors, Adv. Funct. Mater. 32 (33) (2022) 2204565, https://doi.org/10.1002/adfm.202204565.
[30] J. Lyu, Q. Zhou, H. Wang, Q. Xiao, Z. Qiang, et al., Mechanically strong, freeze-resistant, and ionically conductive organohydrogels for flexible strain sensors and batteries, Adv. Sci. 10 (9) (2023) 2206591, https://doi.org/10.1002/advs.202206591.
[31] J.Y. Li, Q.L. Ding, H. Wang, Z.X. Wu, X.C. Gui, et al., Engineering smart composite hydrogels for wearable disease monitoring, Nano-Micro Lett. 15 (1) (2023) 105, https://doi.org/10.1007/s40820-023-01079-5.
[32] Y. Zheng, A. Baidya, N. Annabi, Molecular design of an ultra-strong tissue adhesive hydrogel with tunable multifunctionality, Bioac. Mater. 29 (2023) 214–229, https://doi.org/10.1016/j.bioactmat.2023.06.007.
[33] C. Fu, L. Shen, L. Liu, P. Tao, L. Zhu, et al., Hydrogel with robust dhesion in various liquid environments by electrostatic-induced hydrophilic and hydrophobic polymer chains migration and rearrangement, Adv. Mater. (2023) 2211237, https://doi.org/10.1002/adma.202211237.
[34] P. Ma, W. Liang, R. Huang, B. Zheng, K. Feng, et al., Super-structured wet-adhesive hydrogel with ultralow swelling, ultrahigh burst pressure tolerance, and anti-postoperative adhesion properties for tissue adhesion, Adv. Mater. 36 (11) (2023) 2305400, https://doi.org/10.1002/adma.202305400.
[35] B. Yi, T.J. Li, B.G. Yang, S.R. Chen, J.Y. Zhao, et al., Surface hydrophobization of hydrogels via interface dynamics-induced network reconfiguration, Nat. Commun. 15 (1) (2024) 239, https://doi.org/10.1038/s41467-023-44646-5.
[36] J.-C. Hsieh, W. He, D. Venkatraghavan, V.B. Koptelova, Z.J. Ahmad, et al., Design of an injectable, self-adhesive, and highly stable hydrogel electrode for sleep recording, Device 2 (2) (2024) 100182, https://doi.org/10.1016/j.device.2023.100182.

[37] S. Jin, H. Choi, D. Seong, C.L. You, J.S. Kang, et al., Injectable tissue prosthesis for instantaneous closed-loop rehabilitation, Nature 623 (7985) (2023) 58–65, https://doi.org/10.1038/s41586-023-06628-x.
[38] S. Kim, J. Jang, K. Kang, S. Jin, H. Choi, et al., Injection-on-skin granular adhesive for interactive human-machine interface, Adv. Mater. 35 (48) (2023) 2307070, https://doi.org/10.1002/adma.202307070.
[39] K. Park, K. Kang, J. Kim, S.D. Kim, S. Jin, et al., Balanced coexistence of reversible and irreversible covalent bonds in a conductive triple polymeric network enables stretchable hydrogels with high toughness and adhesiveness, ACS Appl. Mater. Interfaces 14 (50) (2022) 56395–56406, https://doi.org/10.1021/acsami.2c17676.
[40] X. Zhou, A. Rajeev, A. Subramanian, Y. Li, N. Rossetti, et al., Self-healing, stretchable, and highly adhesive hydrogels for epidermal patch electrodes, Acta Biomater. 139 (2022) 296–306, https://doi.org/10.1016/j.actbio.2021.07.069.
[41] L. Zhang, S.H. Wang, Z.M. Wang, Z. Huang, P.H. Sun, et al., A sweat-pH-enabled strongly adhesive hydrogel for self-powered e-skin applications, Mater. Horiz. 10 (6) (2023) 2271–2280, https://doi.org/10.1039/D3MH00174A.
[42] Y.Q. Liu, P.D. Wang, X. Su, L. Xu, Z.L. Tian, et al., Electrically programmable interfacial adhesion for ultrastrong hydrogel bonding, Adv. Mater. 34 (13) (2022) 2108820, https://doi.org/10.1002/adma.202108820.
[43] H.X. Su, Q.T. Li, D.G. Li, H.F. Li, Q. Feng, et al., A versatile strategy to construct free-standing multi-furcated vessels and a complicated vascular network in heterogeneous porous scaffolds combination of 3D printing and stimuli-responsive hydrogels, Mater. Horiz. 9 (9) (2022) 2393–2407, https://doi.org/10.1039/d2mh00314g.
[44] L. Tang, D. Zhang, L. Gong, Y.X. Zhang, S.W. Xie, et al., Double-network physical cross-linking strategy to promote bulk mechanical and surface adhesive properties of hydrogels, Macromolecules 52 (24) (2019) 9512–9525, https://doi.org/10.1021/acs.macromol.9b01686.
[45] Y.W. Zhang, Y. Dai, F. Xia, X.J. Zhang, Gelatin/polyacrylamide ionic conductive hydrogel with skin temperature-triggered adhesion for human motion sensing and body heat harvesting, Nano Energy 104 (2022) 107977, https://doi.org/10.1016/j.nanoen.2022.107977.
[46] X.Q. Yan, Q. Chen, L. Zhu, H. Chen, D.D. Wei, et al., High strength and self-healable gelatin/polyacrylamide double network hydrogels, J. Mater. Chem. B 5 (37) (2017) 7683–7691, https://doi.org/10.1039/c7tb01780d.
[47] X. Du, L. Yang, N. Liu, Recent progress on poly(3,4-ethylenedioxythiophene):poly (styrenesulfonate) bioelectrodes, Small Sci. 3 (7) (2023) 2300008, https://doi.org/10.1002/smsc.202300008.
[48] M.D. Ferro, N.A. Melosh, Electronic and ionic materials for neurointerfaces, Adv. Funct. Mater. 28 (12) (2017) 1704335, https://doi.org/10.1002/adfm.201704335.
[49] S.M. Wellman, J.R. Eles, K.A. Ludwig, J.P. Seymour, N.J. Michelson, et al., A materials roadmap to functional neural interface design, Adv. Funct. Mater. 28 (12) (2017) 1701269, https://doi.org/10.1002/adfm.201701269.
[50] G.G. Yang, Y.J. Hu, W. Guo, W. Lei, W. Liu, et al., Tunable hydrogel electronics for diagnosis of peripheral neuropathy, Adv. Mater. 36 (18) (2024) 2308831, https://doi.org/10.1002/adma.202308831.
[51] S.-C. Shi, T.-W. Chang, FTIR and Raman study of the structural properties and tribological characteristics of collagen, Opt. Quant. Electron. 50 (12) (2018) 438, https://doi.org/10.1007/s11082-018-1700-0.
[52] F. Polyak, G. Reich, Infrared spectroscopic study of the coil-helix transition of highly concentrated gelatin formulations, Eur. J. Pharm. Biopharm. 140 (2019) 11–19, https://doi.org/10.1016/j.ejpb.2019.04.010.
[53] Y. Liu, H. Li, X. Wang, T. Lv, K. Dong, et al., Flexible supercapacitors with high capacitance retention at temperatures from -20 to 100 °C based on DMSO-doped polymer hydrogel electrolytes, J. Mater. Chem. A 9 (20) (2021) 12051–12059, https://doi.org/10.1039/d1ta02397g.
[54] L. Cheng, J. Li, A.Y. Guo, J.H. Zhang, Recent advances in flexible noninvasive electrodes for surface electromyography acquisition, npj Flex, Electron. 7 (1) (2023) 39, https://doi.org/10.1038/s41528-023-00273-0.
[55] J. Li, Z. Liu, Y. Tang, J. Xian, C. He, et al., An interfacial gel electrode patch with tunable hydrogen bond network for electromyographic sensing and discrimination, CCS Chemistry 6 (2) (2024) 450–464, https://doi.org/10.31635/ccschem.023.202202564.
[56] H.W. Ji, M.Y. Wang, Y.T. Wang, Z.H. Wang, Y.J. Ma, et al., Skin-integrated, biocompatible, and stretchable silicon microneedle electrode for long-term EMG monitoring in motion scenario, npj Flex Electron. 7 (1) (2023) 46, https://doi.org/10.1038/s41528-023-00279-8.
[57] D.K. Song, G. Ye, Y. Zhao, Y. Zhang, X.C. Hou, et al., An all-in-one, bioderived, air-permeable, and sweat-stable MXene epidermal electrode for muscle theranostics, ACS Nano 16 (10) (2022) 17168–17178, https://doi.org/10.1021/acsnano.2c07646.